Identification and characterization of a new Down syndrome model, Ts[Rb(12.17^{16})]2Cje, resulting from a spontaneous Robertsonian fusion between T(17^{16})65Dn and mouse Chromosome 12

Angela J. Villar,[1] Pavel V. Belichenko,[2] Anne Marie Gillespie,[1] Heather M. Kozy,[1] William C. Mobley,[2] Charles J. Epstein[1]

[1]Department of Pediatrics, University of California, San Francisco, San Francisco, California 94143, USA
[2]Department of Neurology, Stanford University Medical Center, Stanford, California 94305, USA

Abstract

The segmental trisomy model, Ts65Dn, has been a valuable resource for the study of the molecular and developmental processes associated with the pathogenesis of Down syndrome. However, male infertility and poor transmission of the small marker chromosome, T(17^{16})65Dn, carrying the distal end of mouse Chromosome 16 (MMU16) are limiting factors in the efficient production of these animals for experimental purposes. We describe here the identification and preliminary characterization of mice, designated Ts[Rb(12.17^{16})]2Cje, carrying a chromosomal rearrangement of the Ts65Dn genome whereby the marker chromosome has been translocated to Chromosome 12 (MMU12) forming a Robertsonian chromosome. This stable rearrangement confers fertility in males and increases the frequency of transmitted segmental trisomy through the female germline. We confirm retention of a dosage imbalance of human Chromosome 21 (HSA21)-homologous genes from *App* to the telomere and expression levels similar to Ts65Dn within the triplicated region. In addition, we characterized the dendritic morphology of granule cells in the fascia dentata in Ts[Rb(12.17^{16})]2Cje and 2N control mice. Quantitative confocal microscopy revealed decreased spine density on the dendrites of dentate granule cells and significantly enlarged dendritic spines affecting the entire population in Ts[Rb(12.17^{16})]2Cje as compared to 2N controls. These findings document that the structural dendritic spine abnormalities are similar to those previously observed in Ts65Dn mice. We conclude that this new model of Down syndrome offers reproductive advantages without sacrificing the integrity of the Ts65Dn model.

Down syndrome (DS), or trisomy 21 (Ts21), is the most common nonheritable cause of mental retardation among humans, occurring at a rate of 1 in 700 live births (Pulsifer 1996). The consequence of Ts21 is a chromosome imbalance that results in diverse physical and developmental abnormalities. Research on the identification of genetic factors contributing to this disease and on the molecular basis of specific pathologies stimulated the development of various mouse trisomic models. The first segmental trisomy model, Ts65Dn, is aneuploid (41 chromosomes) and has a small translocation or marker chromosome composed of the centromeric region of Chromosome 17 (MMU17) and a portion of MMU16 containing a region orthologous to HSA21. The trisomic segment of MMU16 in Ts65Dn mice corresponds to a portion of HSA21 that spans 15.6 Mb and contains about 108 of the 225–250 genes in the HSA21 gene catalog (Hattori et al. 2000). Therefore, with the exception of the genes distal to *Mx* in HSA21q22.3, the genetic insult in these mice corresponds closely to that of Ts21 in humans (Reeves et al. 1995). Ts65Dn mice transmit the extra, freely segregating chromosome through the female germline (Davisson et al. 1993; Reeves et al. 1995), but males are infertile, probably because of spermatogenic arrest in metaphase I owing to the presence of the extra chromosome.

Correspondence to: Angela J. Villar; E-mail: avillar@itsa.ucsf.edu

Here we report the identification of a new model of DS that was spontaneously derived from a natural mating between a Ts65Dn female and a diploid B6EiC3SnF1 male. Combined cytogenetic, fluorescence *in situ* hybridization (FISH), and molecular analyses were used to identify a founder female. Chromosome analysis revealed a Robertsonian fusion between the translocation chromosome T(17^{16})65Dn, from the reciprocal translocation T(17A2;16C3–4)65Dn, and MMU12. Quantitative polymerase chain reaction (PCR), which is widely used for identifying genomic copy number changes (Ruiz-Ponte et al. 2000; Wilke et al. 2000), confirmed triplication of the genes from *App* to *Mx1* and increased expression of the genes in this region in a quantitative range similar to Ts65Dn. This model of DS, designated "Ts[Rb(12.17^{16})]2Cje," produces fertile males; and females transmit the Robertsonian translocation at twice the frequency compared with the transmission of the freely segregating extra 17^{16} chromosome in the Ts65Dn.

Previously, we reported that granule cells of the fascia dentata of Ts65Dn mice demonstrate a decreased density of spines on the dendrites, enlargement of the spine head, and decreased length of the spine neck (Belichenko et al. 2004). Here, we report that Ts[Rb(12.17^{16})]2Cje mice exhibit neurological features comparable with those of Ts65Dn mice, thereby validating the utility of this segmental trisomy model for the study of the molecular, genetic, and developmental mechanisms underlying DS.

Materials and methods

Genotyping. Ts65Dn and Ts[Rb(12.17^{16})]2Cje mice were obtained by mating female carriers of the T(17^{16})65Dn marker chromosome and Rb(12.17^{16}) 2Cje, respectively, with (C57BL/6JEi × C3H/HeS-nJ)F1 (JAX No. JR1875) males at each generation (Davisson et al. 1993). Cultured tail fibroblasts were used for karyotype analysis of metaphase spreads to determine the genotype of each animal according to conventional methods. Ts1Cje<*Sod1a/a*> animals were obtained by mating Ts1Cje<*Sod1a/a*> animals with C57BL/6J<*Sod1a/a*>. Ts1Cje<*Sod1a/c*> animals were derived from a cross between C57BL/6J<*Sod1a/a*> and mice with the balanced translocation, T(12;16)1Cje<*Sod1c/-*>. Because the trisomic segment of MMU16 in Ts1Cje contains a mutated superoxide dismutase (*Sod1*) gene disrupted by a neomycin resistance gene sequence, screening of mice was performed by using multiplex PCR primers for *Neo* and glutamate receptor, ionotropic, kainate 1 (*Grik*) (internal control) as previously described (Sago et al. 1998). All mice were housed 3–5 per cage with a 12-h light–dark cycle and *ad libitum* access to food and water. All animal experiments conducted were performed in accordance with the National Institutes of Health guidelines for the care and use of animals and with protocols approved by the Committee on Animal Research of the University of California, San Francisco, or the Stanford University Institutional Animal Care and Use Committee.

Fertility and segregation analysis. The founder Ts[Rb(12.17^{16})]2Cje and subsequent female progeny carrying the Robertsonian chromosome were bred to (C57BL/6JEi × C3H/HeSnJ)F1 males. To assess fertility, Ts[Rb(12.17^{16})]2Cje males and CD1 females were housed in individual cages and the average numbers of pups per litter were recorded. Fecundity of both males and females was assessed based on the number of pups per litter weaned at 21 days. Germline transmission of T(17^{16})65Dn and Rb(12.17^{16})2 Cje for Ts65Dn and Ts[Rb(12.17^{16})]2Cje, respectively, was determined using genotype data collected from both colonies during the same period of time. Transmission efficiency was determined as the percentage of Ts65Dn and Ts[Rb(12.17^{16})]2Cje animals produced out of the total number of genotyped progeny from their respective colonies.

Histology. Histological studies on testes from 8–11-week-old Ts65Dn, Ts[Rb(12.17^{16})]2Cje, and 2N control males were carried out. After weighing, the organs were fixed in Bouin's solution at 4°C for 24 h. Dehydration of tissues was done in a series of ascendhing concentrations of ethanol for a period of 2–5 h. The tissues were embedded in paraffin and 5-μm sections were cut. Sections were stained with hematoxylin and eosin, mounted with dextran plasticizer xylene, and examined using light microscopy.

Metaphase preparation and FISH analysis. Ts65Dn and Ts[Rb(12.17^{16})]2Cje fetal fibroblasts were grown in Dulbecco's modified Eagle's medium (DMEM) supplemented with 10% fetal bovine serum (FBS). Metaphase chromosomes for G-banding and FISH were prepared as follows: Cells were incubated in medium containing 0.1 μg/ml colchicine (Sigma) for 30 min, lysed at 37°C for 15 min in 0.56% KCl, and fixed in methanol:acetic acid (3:1). G-banding to identify the translocation partner chromosome was performed using the protocol of Davisson and Akeson (1987). FISH was performed using biotin-labeled MMU16- and MMU12-specific paints and FITC-labeled MMU17-specific chromosome paint, singly or in combination, to identify the marker chromosome T(17^{16})65Dn and confirm the translocation partner

Table 1. Primers and probes used for quantification of gene copy number.

	Primers 5′-3′	Probe 5′-3′
App	AACTTGCCCAAAGCTGACAAG	TATCCAGGTAACACCCCGGTCCCA
	TGGCATGTTCTGTCTGGTGTAG	
Sod1	GGACCTCATTTTAATCCTCACTCTAAG	CATGGTGGCCCGGCGGA
	CGTGCTGCTCACCTCTCTTC	
Sim2	TGGACAAAGCGTCCATCATC	ACCAGCTACCTGAAGATGCGCG
	CCTCACCTTCCGGGAAGAC	
Dyrk1a	TTTGGACAGAATGGAGCTATGG	CGTTAATTTGACCGTCTACTCCAATCCCC
	TCCAGCTATGCCAGTCTCTTG	
Mx1	TGCCAAATTCTCCGATTAACC	TCC TGG TCG CTG TGC AAT GAT CC
	AAGGCAACGTTCTGACATAAGG	
β-actin	CCGGGTAACCCTTCTCTTTG	CCAGCTTCTCAGCCACGCCCT
	CGGCAGAAGAAAGACAATTGAG	

MMU12. Hybridization and detection were carried out according to the protocol provided with the StarFish hybridization and detection kits (Cambio, Cambridge, UK). Briefly, after hybridization with a biotin probe, the chromosome spreads were treated with Texas-red avidin and the signals were amplified with biotinylated goat antiavidin followed by Texas-Red avidin. After hybridization with FITC probes, the signals were amplified with rabbit anti-FITC followed by FITC goat antirabbit IgG. An Axioplan II fluorescence microscope (Zeiss) equipped with filter sets for DAPI, FITC, and Texas Red was used for visualizing the metaphase FISH slides. Photographs were digitally captured using Spot Software v2.1 (Diagnostic Instruments, Inc.).

Q-PCR analysis of DNA. Q-PCR assays of genomic DNA were performed using gene-specific fluorescently labeled TaqMan probes in an ABI Prism® Model 7700 Sequence Detector (Applied Biosystems, Foster City, CA) to determine the gene copy numbers of amyloid beta A4 protein precursor (*App*), superoxide dismutase (*Sod1*), single-minded homolog 2 (*Sim2*), dual-specificity tyrosine-phosphorylation regulated kinase 1A (*Dyrk1a*), and interferon-induced GTP-binding protein(*Mx1*). Total brain DNA was extracted from a random sampling of Ts65Dn, Ts[Rb(12.17[16])]2Cje, TslCje, and 2N control adult males according to the manufacturer's protocol (Qiagen, Valencia, CA). Approximately 50 ng of genomic DNA was used as a template in each Q-PCR reaction. The selection of primers and probes was performed using ABI PrimerExpress[TM] software (Applied Biosystems), based on optimal conditions for real-time PCR primer design (Table 1). Primers and probes were obtained from Biosearch Technologies, Inc. (Novato, CA). The PCR amplification profile included an initial incubation at 95°C for 10 min. and 40 cycles of 95°C for 15 sec and 60°C for 1 min using the TaqMan universal PCR Master Mix

kit (Applied Biosystems) under optimized conditions (Table 2). TaqMan PCR was performed in triplicate at least 3 times for each sample. To standardize the quantitation of the selected genes, β-actin was analyzed on each assay plate together with the selected genes of interest. PCR efficiency was determined by running serial dilutions of DNA with each probe ($2 \times$ dilutions, 5 dilutions total). Standard curves for each probe were made by plotting the log input DNA versus the threshold cycle (Ct) value. The slope of the standard curve was used to calculate the PCR efficiency, using $10^{-1/m}-1$. The threshold was set in the linear range of normalized fluorescence, and threshold cycle was measured in each well. Results were analyzed using ABI Sequence Detector software, and the relative copy number of target sequences in each DNA sample was determined using a comparative Ct ($\Delta\Delta Ct$) method (Livak 1997). This method calculates a value relative to both the normal control DNA and to the endogenous control β-actin sequence.

cDNA expression analysis. TaqMan real-time reverse transcriptase PCR (RT-PCR) was carried out using Assays-on-Demand[TM] Gene Expression primer and probe sets (Applied Biosystems) in a 7700 Sequence Detector. Prior to real-time PCR analysis, total brain RNA was isolated from a random sampling of 2N control, Ts65Dn, and Rb(12.Ts65Dn)lCje animals at postnatal day 7 with the use of a com-

Table 2. Optimized primer and probe concentrations for quantification of gene copy number

Gene	Primer	Probe	PCR efficiency
App	900 nm	200 nm	0.986
Dyrk1a	900 nm	200 nm	1.015
Sod1	600 nm	200 nm	0.974
Mxl	600 nm	200 nm	0.986
Sim2	900 nm	200 nm	0.983
β-actin	300 nm	150 nm	0.990

mercial kit (RNeasy mini kit, Qiagen). Each RNA preparation was reverse transcribed according to the manufacturer's protocol (Invitrogen, San Diego, CA), and one-tenth of the mixture was used in the Q-PCR expression analysis of Amyloid beta A4 protein precursor (App), Dual-specificity-tyrosine-phosphorylation regulated kinase 1A (Dyrk1a), Down syndrome cell adhesion molecule (Dscam), Purkinje cell protein 4 (Pcp4), Down syndrome critical region (Dscr1, Dscr2, Dscr3, Dscr6), and E26 avian leukemia oncogene 2 (Ets2). In addition, HPRT was used as the endogenous control on each assay plate to quantify the relative value of their respective message levels. All probes are designed to span exon junctions in the fully processed message in order to prevent reporting of amplification of any possible contaminating genomic DNA. Data were analyzed as described above. Student's t-test was used to determine the significance of any difference in gene expression between Ts65Dn, Ts[Rb(12.17^{16})]2Cje, and 2N control samples. A p-value of < 0.05 was considered significant.

Brain tissue preparations. Three pairs of male 2N control and Ts[Rb(12.17^{16})]2Cje mice were examined at 10–11 months of age. Mice were deeply anesthetized with sodium pentobarbital (200 mg/kg IP) (Abbott Laboratories, North Chicago, IL) and transcardially perfused for 1 min with 0.9% sodium chloride (10 ml) and then for 10 min with 4% paraformaldehyde in 0.1 M phosphate buffered saline (PBS), pH 7.4 (100 ml). After perfusion, brains were removed immediately and placed in 0.1 M PBS. Brains were then sectioned coronally (200 μm thick) on a Vibratome (Series 1000, TPI Inc., St. Louis, MO), and the sections were placed in 0.1 M PBS.

Lucifer yellow microinjection. Lucifer yellow (LY) injections were performed on lightly fixed vibratome slices, as described (Belichenko and Dahlström 1995). In brief, a 200-μm-thick slice was floated onto a glass plate and held in place by a Millipore filter (Millipore Corporation, Billerica, MA) with a small window to allow for visualization of the tissue. The preparation was placed in a petri dish, immersed in PBS, and this "injection chamber" was then transferred to a fluorescence microscope (Nikon Eclipse E800, Japan) equipped with a micromanipulator and source of constant current (1.5-V battery, Duracell, Bethel, CT). Glass microelectrodes (1.2 mm o.d., 0.94 mm i.d., Sutter Instrument Co, Novato, CA) were filled with a 6% aqueous solution of LY CH dilithium salt (Sigma, St. Louis, MO). After penetrating the cell body with the microelec-

trode, LY was iontophoretically injected with negative constant current of 2–5 nA over 5 min, during which time it could be observed to fill the dendrites. About 15–30 individual dentate granule cells were injected in both sides of a brain slice. Injected slices were mounted on a microscope glass slide and coverslipped with 90% glycerol in PB.

Confocal microscopy. Cells labeled with LY were examined and scanned in a Radiance 2000 confocal microscope (BioRad, Hertfordshire, UK) attached to a Nikon Eclipse E800 fluorescence microscope. The laser was an argon/krypton mixed gas laser with the excitation wavelength for LY (488 λ). LaserSharp software (BioRad) was used to establish optimal conditions for collecting images.

The morphology of LY-injected neurons and their spines was studied under the following optimal conditions: the objective lens was 60 × (Nikon; Plan Apo 60 × /1.40 oil); the laser power was 10%; the optical sections were scanned at regular increments of 0.5 μm; the zoom factor was 10; scanning was at 500 lines/sec; each optical section was the result of 3 scans followed by Kalman filtering; pixel size was 0.04 × 0.04 μm; the size of the image was 512 × 512 pixels (i.e., 20 × 20 μm). Each image was saved as a stack of individual optical sections and as a z-projection.

Image analysis. To measure the length of dendrites, count the number of dendritic spines, and estimate the size of heads and the length of necks, the z-projection image of individual dendrites was examined using LaserPix software (BioRad, UK). The number of spines was calculated per 100-μm length of dendrite. Statistical analysis used Student's t-test, and p < 0.05 were considered to be significant. Frequency tables were produced by using Statistica StatSoft software (Tulsa, OK). The reported data are based on analysis of 73 dendrites of dentate granule cells in 2N control mice and 66 dendrites in Ts[Rb(12.17^{16})]2Cje mice.

Results

Identification of the translocation. A female with 40 chromosomes and 41 arms was detected by chromosome analysis of progeny from the Ts65Dn breeding colony (Fig. 1). This female had a unique bi-armed chromosome that appeared to be the result of a fusion between an acrocentric chromosome and the marker chromosome T(17^{16})65Dn, characteristic of Ts65Dn mice. G-banding revealed the translocation partner chromosome to be MMU12 (data not shown). FISH analysis using different combinations
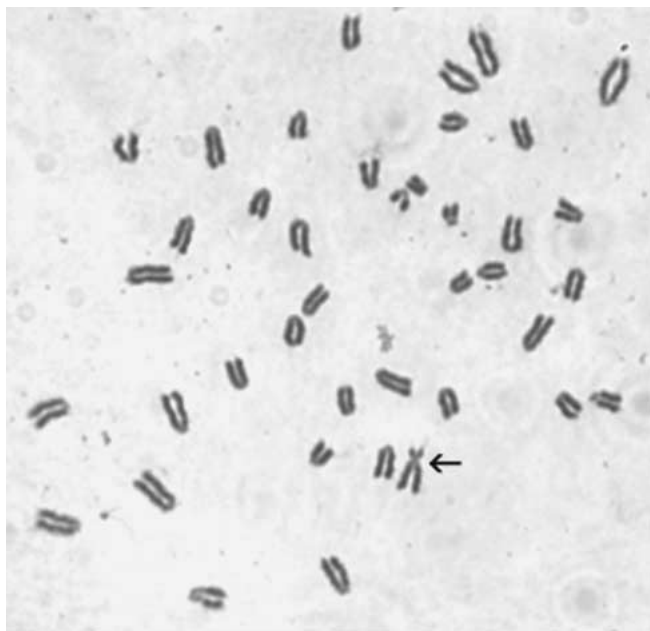
Fig. 1. Ts[Rb(12.17^{16})]2Cje metaphase stained with Giemsa showing the Robertsonian translocation chromosome (arrow), $N = 40$ chromosomes and 41 chromosome arms.

of mouse chromosome paints for MMU16, MMU17, and MMU12 demonstrated that the small acrocentric 17^{16} translocation chromosome of Ts65Dn had fused to MMU12, resulting in a Robertsonian fusion chromosome (Fig. 2).

Fertility and segregation. To assess fertility and the frequency of transmission of the Robertsonian chromosome, the founder female was bred to a (C57BL/6JEi×C3H/HeSnJ)F1 male (the same genetic background that is used in breeding Ts65Dn mice). The founder female produced 7 litters with an average litter size of 6.2 pups/litter. Transmission frequency ranged from 33% to 60% with an average of 45% over the founder's reproductive lifespan. Transmission frequencies for all subsequent Ts[Rb(12.17^{16})]2Cje breeding females were compared with those observed in the Ts65Dn colony over the same period of time. Whereas litter sizes were similar between the two types of breeding females, the frequency of progeny inheriting the Robertsonian chromosome was significantly higher than the frequency of progeny inheriting the freely segregating T(17^{16})65Dn chromosome. A total of 18 Ts[Rb(12.17^{16})]2Cje females produced 40 litters compared with 43 litters produced by 21 Ts65Dn females with an average litter size of 5.4 pups/litter in both colonies. Production of segmental trisomics in the Ts[Rb(12.17^{16})]2Cje and Ts65Dn colonies was 43% and 24%, respectively. Transmission of Rb(12.17^{16})2Cje ranged from 0%

(5/40 litters) to 100% (3/40 litters) in the Ts[Rb(12.17^{16})]2Cje colony with an average of 43%, whereas transmission of T(17^{16})65Dn ranged from 0% (16/43 litters) to 75% (2/43 litters) in the Ts65Dn colony, effectively reducing the production of trisomics to 24%. Furthermore, Ts[Rb(12.17^{16})]2Cje males were as fertile as the females (data not shown), although they transmitted the Robertsonian chromosome at a rate of only 1%–5%.

Like Ts65Dn mice, Ts[Rb(12.17^{16})]2Cje mice are about 20% smaller in size postnatally compared with 2N control littermates, and this smaller size persists throughout life.

Histological analysis of the testis. All morphological analyses were based on evaluation of at least 3 mice for each genotype group at the age of 8 weeks. The weights of Ts65Dn (37.4 ± 1.6 mg) (±SD) and Ts[Rb(12.17^{16})]2Cje (64.6 ± 8.3 mg) testes were 37.9% and 65.6% of 2N control testes (98.4 ± 8.3 mg), respectively. Histological analysis of testes from Ts65Dn showed that spermatocytes beyond the pachytene stage and round spermatids were significantly reduced in number. Elongated spermatids were rare, and the few remaining spermatids had deformed nuclei. Some germ cells appeared to be detached from the few visible Sertoli cells (SC), and Leydig cells (LC) appeared loosely clustered within an expanded interstitial compartment (Fig. 3B). In contrast, the Ts[Rb(12.17^{16})]2Cje testes (Fig. 3C) were structurally indistinguishable from the 2N controls (Fig. 3A) and had a normal progression of spermatogenesis.

Gene copy number and expression levels. To determine whether the Ts[Rb(12.17^{16})]2Cje model is truly trisomic for genes corresponding to those on HSA21q21–22.3, we analyzed gene copy number as measured by Q-PCR. As predicted, both Ts65Dn and Ts[Rb(12.17^{16})]2Cje had gene copy number ratios relative to 2N controls that were very close to 1.5 for *App, Sod1, Sim2, Dyrk1a,* and *Mx1* (Fig. 4). For comparison, we also examined Ts1Cje<*Sod1*a/a>, another model for Down syndrome (Sago et al.1998). These mice are trisomic for a smaller region of MMU16, from *Sod1* to *Mx1*, as a result of a chromosome rearrangement in which a portion of MMU16 has translocated onto MMU12. Ts1Cje animals, however, are not functionally trisomic for *Sod1* because this gene is disrupted by the neomycin resistance sequence introduced at the time that the translocation giving rise to them occurred. Q-PCR confirmed that Ts1Cje segmental trisomics are diploid for *App and Sod1*, with a gene copy number ratio of 1.0 relative to 2N controls. Although the
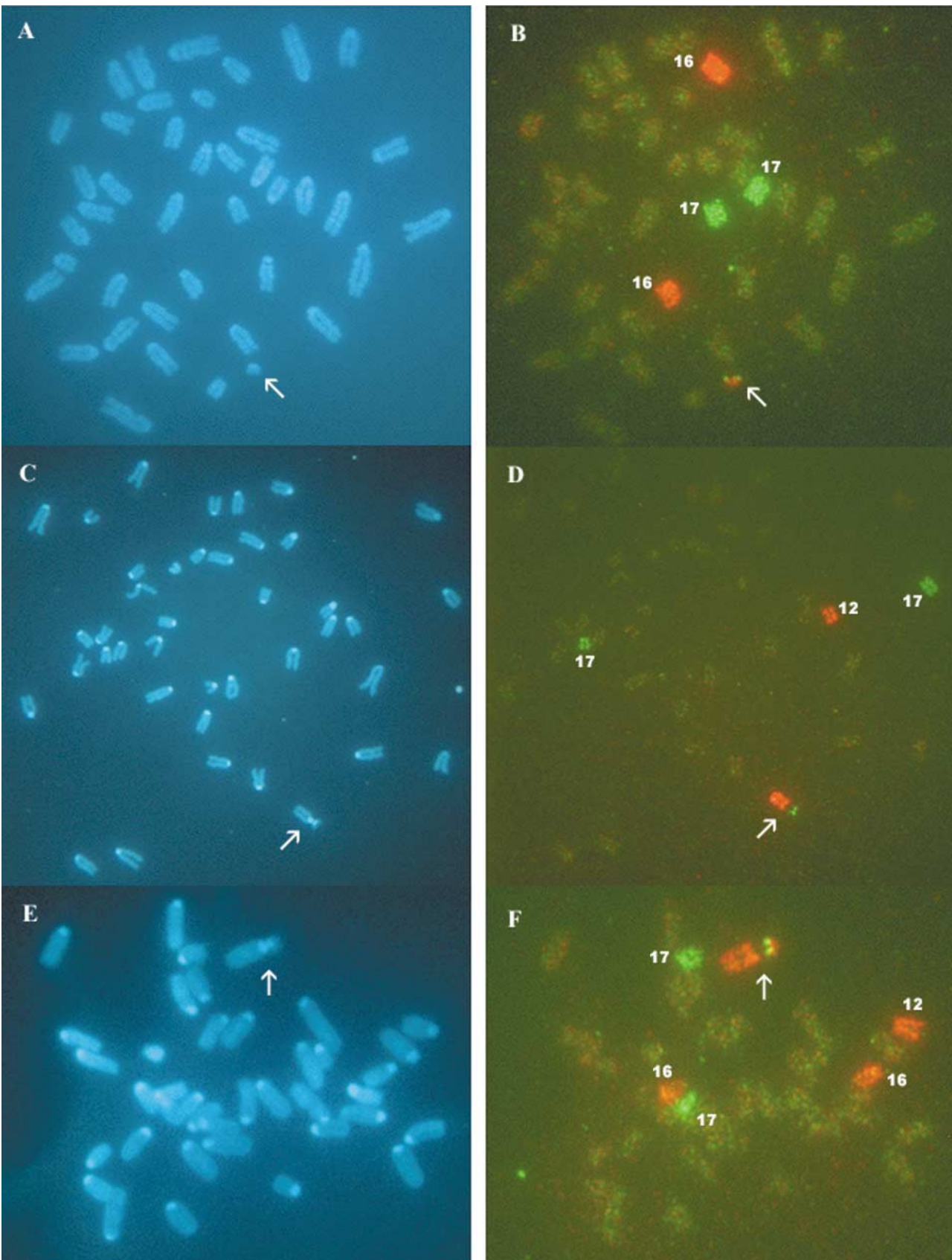
Fig. 2. Metaphase spreads from cultured embryonic fibroblasts. (**A**) and (**B**) Ts65Dn; (**C**)–(**F**) Ts[Rb(12.17^{16})]2Cje. The chromosomes **A**, **C**, and **E** are visualized with the DAPI counterstain. (**B**) MMU16s are painted with a biotin probe (red) and MMU17s with a FITC probe (green). The translocation chromosome, T(17^{16})65Dn, is indicated with an arrow. (**D**) MMU12s are painted with a biotin probe and MMU17s with a FITC probe. (**F**) MMU12s and MMU16s are painted with biotin probes and MMU17s with a FITC probe. (**C**)–(**F**) The Robertsonian translocation chromosome, which is composed of
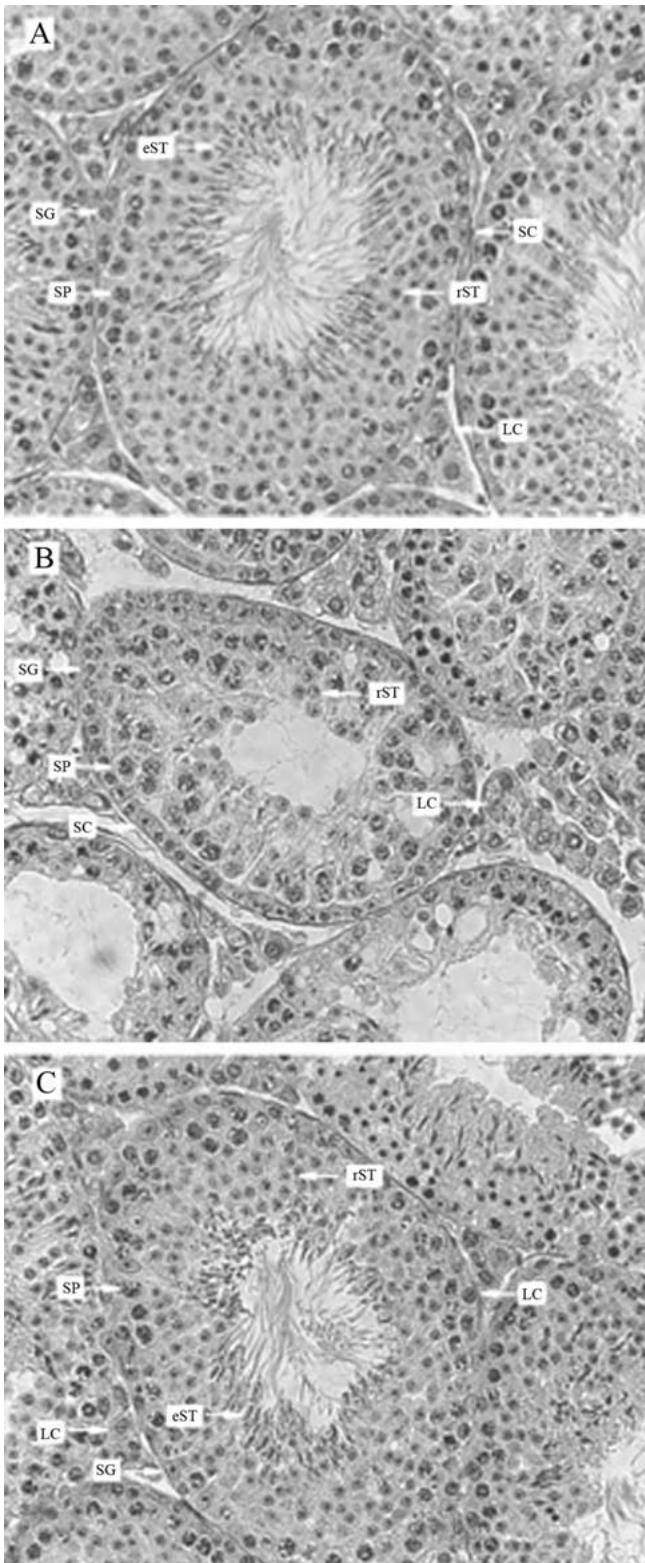
Fig. 3. Histology of testes from Ts65Dn, Ts[Rb(12.17^{16})]2Cje, and 2N control mice stained with H&E. (**A**)–(**C**) Testis sections were prepared from 8-week-old mice. (**A**) Testis from a normal littermate. Closely packed seminiferous tubules [containing spermatogonia (SG), spermatocytes (SP), round spermatids (rST), and elongated spermatids (eST)], a limited interstitial compartment (LC), and complete spermatogenesis as supported by abundance of elongated spermatids were observed. (**B**) Testis from an infertile Ts65Dn mouse. Note reduction of spermatocytes beyond the pachytene stage and of round spermatids and absence of elongated spermatids. (**C**) Testis from fertile Ts[Rb(12.17^{16})]2Cje mouse showing the normal progression of spermatogenesis. SC-Sertoli cells, LC-Leydig cell.

lele because of the presence of a single-base-pair polymorphism. Therefore, when gene copy analysis was performed on genomic DNA from Ts1Cje<Sod1a/c> animals, ratios of 1.0 and 0.5 were observed for *App* and *Sod1*, respectively (Fig. 5).

To determine whether genes in the triplicated region of MMU16 are expressed at increased levels as a reflection of their increased dosage, we performed TaqMan real-time RT-PCR using RNA from day 7 brains. Similar to a recent report (Lyle et al. 2004), expression analyses demonstrated that genes in the triplicated region were expressed at significantly higher levels in the Ts[Rb(12.17^{16})]2Cje brain compared with 2N controls and were again in the vicinity of 1.5 × control levels (Fig. 6). Furthermore, the increased levels of gene expression were not significantly different from Ts65Dn.

Histological analysis of the brain. We previously described several morphological phenotypic features on dentate granule cells that were distinct between 2N control and Ts65Dn mice (Belichenko et al. 2004). The most consistent differences were noted in the fascia dentata, where there were significant decreases in spine density on dendrites of Ts65Dn granule cells and dendritic spines were significantly enlarged. However, there were no changes in dendritic width between 2N control and Ts65Dn mice. In the present study, we examined the same phenotypic features in Ts[Rb(12.17^{16})]2Cje and 2N control mice to determine whether Ts65n and Ts[Rb(12.17^{I6})]2Cje mice were comparable. To define the morphology of dendrites and dendritic spines, we microinjected LY into individual dentate granule cells in brain slices from 2N control and Ts[Rb(12.17^{16})]2Cje mice. The dendrites of injected neurons were analyzed by quantitative confocal microscopy.

Spine density is significantly reduced in Ts[Rb(12.17^{16})]2Cje mice dentate granule cells. Figure 7 shows representative images of dendrite dentate

primer set for *Sod1* was not intentionally designed to discriminate between the *a* and *c* alleles of this gene, which are used in typing the animals, we discovered that the primers fortuitously amplify only the *a* al-
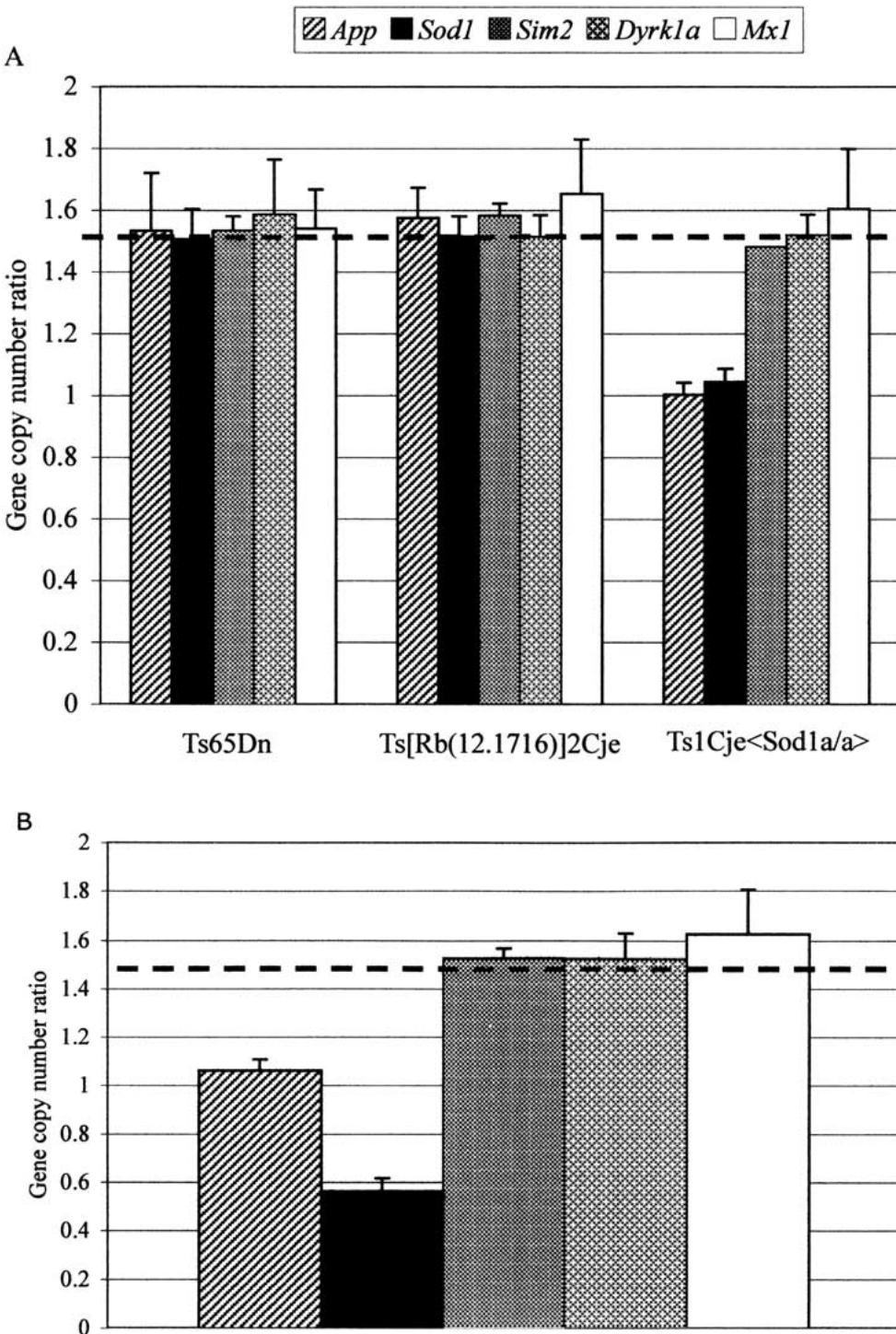
Fig. 4. (**A**) Gene copy number ratio (±SD) for *App*, *Sod1*, *Sim2*, *Dyrk1a*, and *Mx1* in DNA samples from Ts65Dn, Ts[Rb(12.17[16])]2Cje, Ts1Cje<*Sod1a/a*>. Horizontal dashed line represents the position of a relative gene copy number of 1.5. (**B**) Evaluation of gene copy number ratio (±SD) in segmental trisomic DS model Tsl Cje<*Sod1a/c*>, relative to 2N controls using real-tune Q-PCR. Horizontal dashed line represents the position of a relative gene copy number of 1.5.

granule cells in 2N control and Ts[Rb(12.17[16])]2Cje mice. To examine the structure of synapses in Ts[Rb(12.17[16])]2Cje mice, we asked whether there was a change in the density of spines on the dendrites. For this analysis, the number of spines per 100-µm length of dendrite were counted in z-projections of LY-injected dendrites. Spine density was significantly reduced on dendrites of dentate granule cells in an entire molecular layer (Fig. 8). The decreases averaged about 15%. Subdividing fascia den-
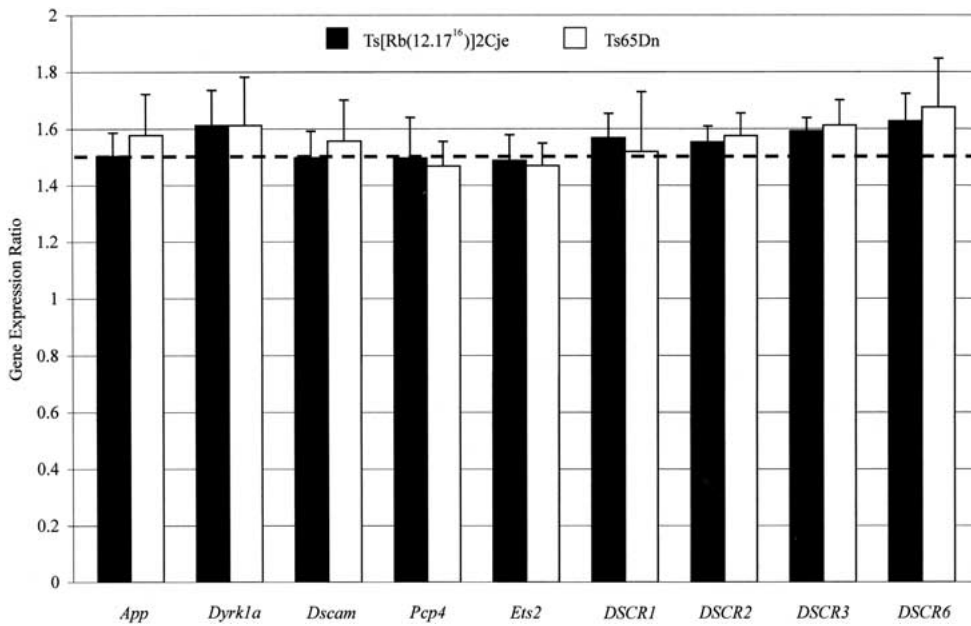
Fig. 5. Evaluation of gene expression levels (±SD) in Ts65Dn and Ts[Rb(12.17^{16})]2Cje ($N = 3$) relative to 2N controls using real-time Q-PCR. Horizontal dashed line represents the position of a relative gene expression level of 1.5.

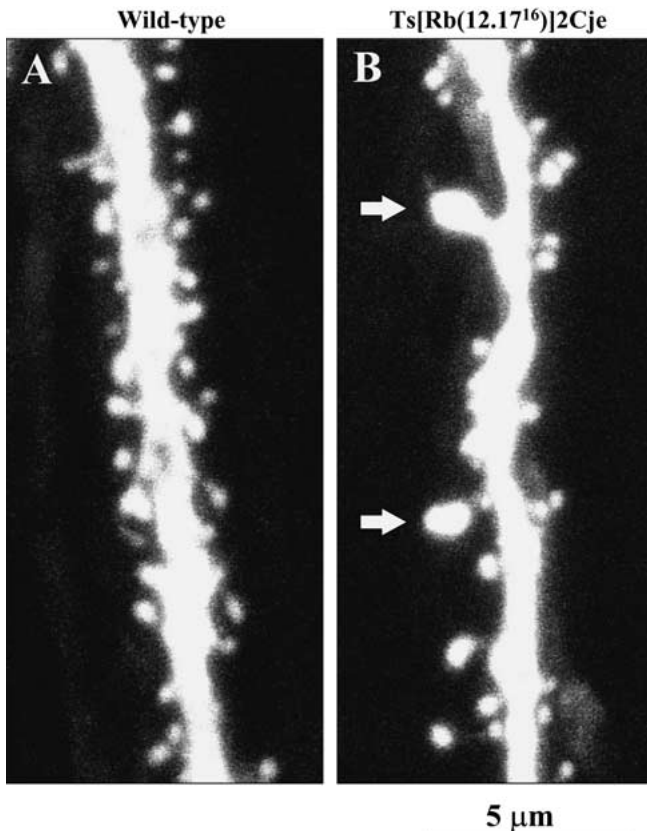tata, the decrease was present throughout the molecular layer and was statistically significant for

Fig. 6. Dendritic spines in molecular layer of fascia dentata. Note enlarged spines in Ts[Rb(12.17^{16})]2Cje mice (arrows) as well as a reduction in their number. Scale bar = 5 μm.

the inner and middle third portions of the molecular layer of the fascia dentata (Fig. 8). There were no differences in the width of the dendrites (i.e., in the inner molecular layer: 2N control = 1.24 +/− 0.02 μm, $n = 73$, Ts[Rb(12.17^{16})]2Cje = 1.22 +/− 0.03 μm, $n = 66$, $p = 0.65$; in the middle molecular layer: 2N control = 1.04 +/− 0.02 μm $n = 51$, Ts[Rb(12.17^{16})]2Cje = 1.04 +/− 0.02 μm, $n = 62$, $p = 0.98$; in the outer molecular layer: 2N control = 0.88 +/− 0.02 μm, $n = 39$, Ts[Rb(12.17^{16})]2Cje = 0.91 +/− 0.02 μm, $n = 56$, $p = 0.49$). We conclude that changes in spine density on dendrites in the fascia distinguish the Ts[Rb(12.17^{16})]2Cje from the 2N control mice.

Dendritic spines are also significantly enlarged in Ts[Rb(12.17^{16})]2Cje. There was a marked increase in the size of dendritic spines in Ts[Rb (12.17^{16})]2Cje mice (Fig. 7, 8A, 8B). The increases averaged about 38%. This was due to an overall increase in spine size (Fig. 8B) that resulted in the presence of many markedly enlarged spines. Arrows on Fig. 7 point to enlarged spines on the dendrites of granule cells in the fascia dentate in Ts[Rb(12.17^{16})]2Cje mice. In our previous study on Ts65Dn mice (Belichenko et al. 2004), we defined enlarged spines as those with a head area bigger than 0.5 μm^2. In the present study, 2N control mice presented only 2% of spines (14/615) with heads bigger than 0.5 μm^2, with no spines with a head area bigger than 0.7 μm^2 In contrast, Ts[Rb(12.17^{16})]2Cje mice with spines larger than 0.5 μm^2 represented approximately 13% (76/564) of the total number. In addition, dendritic spines in Ts[Rb(12.17^{16})]2Cje mice had significantly shorter necks (Fig. 8C and D),
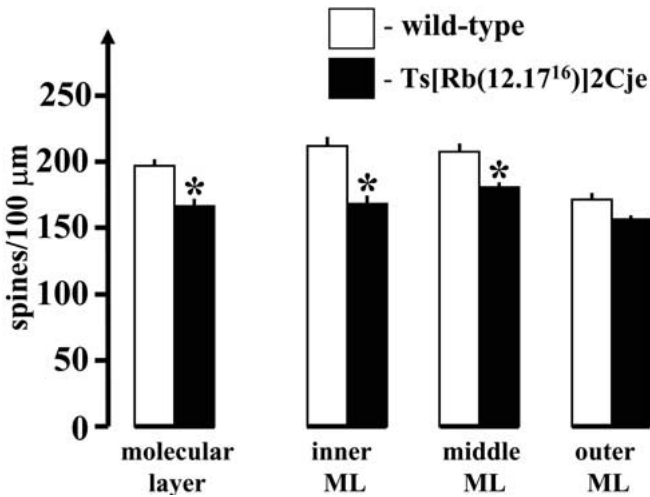
Fig. 7. Quantitative analysis of dendritic spine density on granule cells of the fascia dentata in 2N control (empty bars) and Ts[Rb(12.17[16])]2Cje (black bars) mice. Spine density was measured for the entire molecular layer of the fascia dentata (molecular layer), and in the inner (inner ML), middle (middle ML), and outer (outer ML) third subdivisions. Density is expressed as number of spines per 100-μm length of dendrite. Results are presented as mean +/− SEM; *p < 0.05, significantly different from 2N control mice.
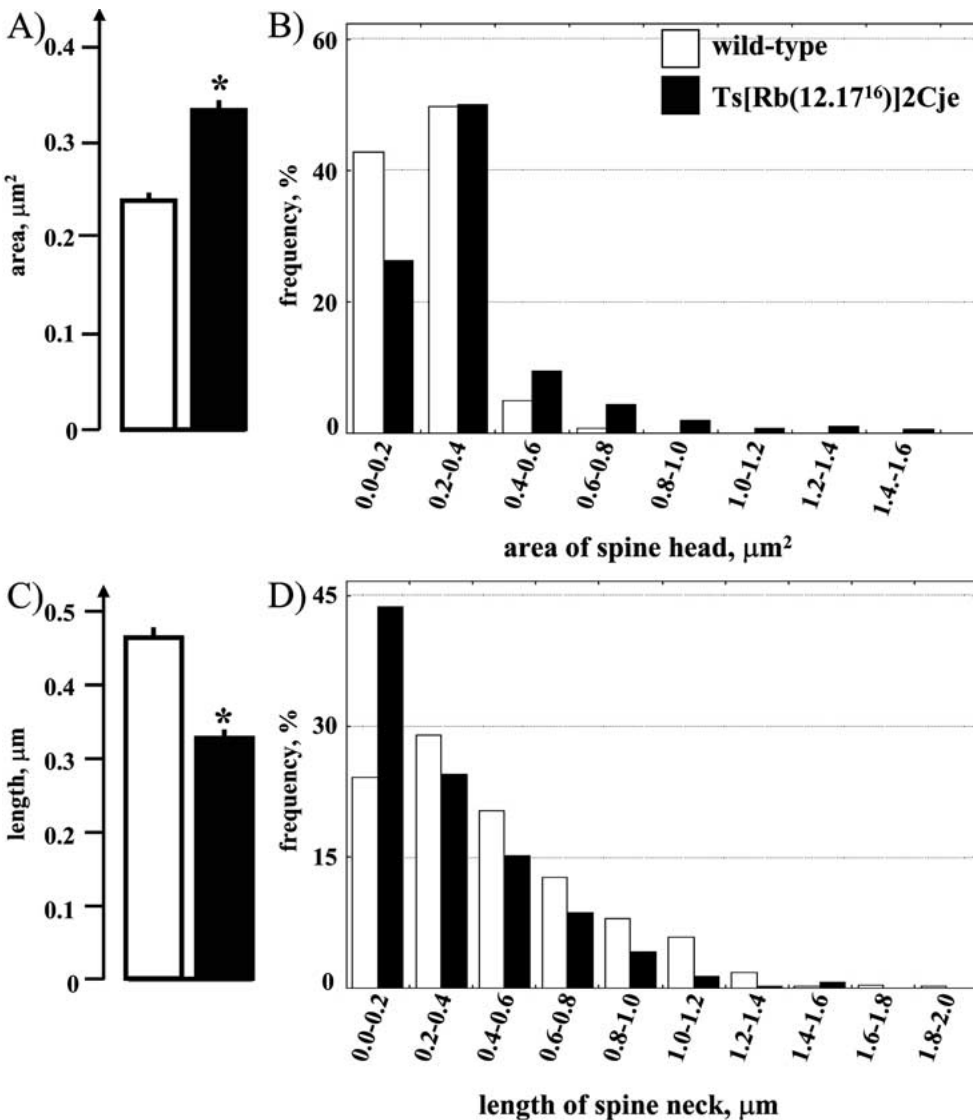

Fig. 8. Quantitative analysis of the area (**A**) and frequency distribution (**B**) of spine head area, length (**C**), and frequency distribution (**D**) of spine neck length in fascia dentata in 2N control (empty bars) and Ts[Rb(12.17[16])]2Cje (black bars) mice. Results are presented as mean +/− SEM. *p < 0.05, significantly different from control.

similar to what was previously reported for Ts65Dn (Belichenko et al. 2004). The decreases averaged about 30% for both DS models. We conclude that changes in morphology of individual spines on dendrites in the fascia dentata distinguish Ts[Rb(12.17[16])]2Cje from 2N control mice and are comparable to the Ts65Dn phenotype.

Discussion

While primates with the genetic and clinical equivalence of trisomy 21 (Ts21) and DS have been observed, they do not offer significant advantages over humans for investigational purposes. Therefore, the mouse has been the model animal of choice for defining the anatomical correlates of human mental retardation and providing a model for the preclinical testing of putative therapies, both of which are relevant to human mental retardation research. Mouse models of DS have been generated and studied with a view of gaining insight into the molecular, genetic, and/or developmental mechanisms that underlie the pathogenesis of one or more of the anomalies that occur in DS. No model can be an exact one, since no other organism duplicates the human with respect to all of his or her biological and genetic attributes. Nevertheless, the Ts65Dn mouse model exhibits many of the phenotypic features of Ts21 and has been widely studied (Davisson et al. 1993; Escorihuela et al. 1995; Reeves et al. 1995; Holtzman et al, 1996; Davisson and Costa 1999). Unfortunately, Ts65Dn mice are difficult to breed, and their poor reproduction is compounded by the fact that they generate segmental trisomy progeny at a rate of only 20%–25%

We have confirmed that the Ts[Rb(12.17[16])]2Cje mouse is genetically equivalent to Ts65Dn. Similar to what has been described in Ts65Dn (Reeves et al. 1995; Akeson et al. 2001), Ts[Rb(12.17[16])]2Cje mice are at a dosage inbalance for genes corresponding to those on HSA21q21-22.3, the region that includes the so-called DS "critical region." Unlike Ts65Dn, however, the Ts[Rb(12.17[16])]2Cje model has two important advantages that make it a valuable resource for scientific investigation: Ts[Rb(12.17[16])]2Cje females produce trisomic offspring at a significantly higher frequency and the males are fertile. While the low frequency of transmission through the male germline prohibits the practical use of trisomic males in Ts[Rb(12.17[16])]2Cje husbandry, male fertility confers the ability to identify epigenetic factors affecting male and female transmission of the trisomic segment, which was heretofore not possible. The Robertsonian chromosome is stable and, to date, has been transmitted through both the male and female germline for five generations.

It is of interest that two of the three translocation chromosomes leading to segmental trisomy of MMU16, T(12;16)1Cje and Ts[Rb(12.17[16])]2Cje, involve MMU16 and MMU12 as translocation partners. Furthermore, Robertsonian translocations involving HSA21 are found in approximately 5% of patients with DS. Interestingly, the most common nonhomologous Robertsonian translocation in DS results in a fusion between 21q and 14q, the human orthologs of the chromosomal region in MMU16 and MMU12, respectively (Berend et al. 2003). The significance of these spontaneous translocation events involving MMU12/MMU16 and HSA14 /HSA21 is presently unknown. It could merely be coincidental, but it might also imply that there is some type of preferential chromosomal association during meiosis, notably that MMU12 and 17 like HSA14 and 21 have ribosomal clusters at their acrocentric ends.

The present study demonstrates the existence of some of the same neurological phenotypic features in Ts[Rb(12.17[16])]2Cje mice as were described previously in the Ts65Dn DS model (Belichenko et al. 2004). We observed a similar significant decrease in the density of dendritic spines of dentate granule cell neurons in Ts[Rb(12.17[16])]2Cje and Ts65Dn mice. The average decrease was 15% and 17% in Ts[Rb(12.17[16])]2Cje mice and Ts65Dn mice, respectively. The spine density was significantly decreased in the inner and middle third subdivisions of the molecular layer but not in the outer third of the molecular layer in both Ts[Rb(12.17[16])]2Cje and Ts65Dn mice compared with their 2N controls. The average area of the spine head increased by 38% and 65% in Ts[Rb(12.17[16])]2Cje and Ts65Dn mice, respectively. Moreover, the length of the spine neck was decreased by 30% and 32% in Ts[Rb(12.17[I6])]2Cje and Ts65Dn mice, respectively.

This study provides genetic expression and histological evidence to support the conclusion that, because of their reproductive advantages, the new Ts[Rb(12.17[16])]2Cje model of DS is a useful alternative to Ts65Dn.

Finally, in addition to karyotype analysis of either blood or cultured tail fibroblasts, TaqMan real-time PCR has proven to be a reliable method as a genotyping strategy based on gene copy number (Liu et al. 2003; Schaeffeler et al. 2003; Boehm et al. 2004). Although we do not advocate the exclusive use of Q-PCR for genotyping, the simplicity and reproducibility of the TaqMan assay offers a new rapid and cost-effective approach to determine gene copy number in aneuploid mouse models. In addition, with the identification of an allele-specific

primer set for *Sod1*, we propose that Q-PCR technology may be a useful alternative to the conventional method of tracking the *a* and *c* isoforms of CuZnSOD (Luche et al. 1997) to distinguish progeny derived from the cross between Ts65Dn females and T(12;16)1Cje males that is used to produce Ms1CjeTs65Dn segmentally trisomic mice (Sago et al.2000).

Acknowledgments

References

1. Akeson EC, Lambert JP, Narayanswami S, Gardiner K, Bechtel LJ, et al. (2001) Ts56Dn–localization of the translocation breakpoint and trisomic gene content in a mouse model for Down syndrome. Cytogenet Cell Genet 93(3–4), 270–276

2. Belichenko PV, Dahlström A (1995) Studies on the 3-dimensional architecture of dendritic spines variocosities in human cortex by confocal laser scanning microscopy and Lucifer yellow microinjections. J Neurosci Methods 57, 55–61

3. Belichenko PV, Masliah E, Kleschevnikov AM, Villar AJ, Epstem CJ, et al. (2004) Synaptic structural abnormalities in the Ts65Dn mouse model of Down syndrome. J Comp Neurol 480, 281–298

4. Berend SA, Page SL, Atkinson W, McCaskill C, Lamb NE, et al. (2003) Obligate short-arm exchange in *de novo* Robertsonian translocation formation influences placement of crossovers in chromosome 21 nondisjunction. Am J Hum Genet 72(2), 488–495

5. Boehm D, Herold S, Kuechler A, Liehr T, Laccone F (2004) Rapid detection of subtelomeric deletion/duplication by novel real-time quantitative PCR using SYBR-green dye. Hum Mutat 23(4), 368–378

6. Davisson MT, Akeson EC (1987) An unproved method for preparing G-banded chromosomes from mouse peripheral blood. Cytogenet Cell Genet 45(2), 70–74

7. Davisson MT, Costa AC (1999) Mouse models of Down syndrome. Mouse Models of Human Genetic Neurological Diseases, Popko, B. New York, Plenum, 297–327

8. Davisson MT, Schmidt C, Reeves RH, Irving NG, Akeson EC, et al. (1993) Segmental trisomy as a model for Down syndrome. In *The Phenotypic Mapping of Down Syndrome and Other Aneuploid Conditions*, Epstein CJ, ed. New York, Wiley-Liss, Vol 384, 117–133

9. Escorihuela RM, Fernandez–Teruel A, Vallina IF, Baamonde C, Lumbreras, et al. (1995) A behavioral assessment of Ts65Dn mice: a putative Down syndrome model. Neurosci Lett 199(2), 143–146

10. Hattori M, Fujiyama A, Taylor TD, Watanabe H, Yada T, et al. (2000) Chromosome 21 mapping and sequencing consortium. The DNA sequence of human chromosome 21. Nature. 405(6784), 311–319

11. Holtzman DM, Santucci D, Kilbridge J, Chua–Couzens J, Fontana DJ, et al. (1996) Developmental abnormalities and age-related neurodegeneration in a mouse model of Down syndrome. Proc Natl Acad Sci USA 93(23), 13333–13338

12. Liu DP, Schmidt C, Billings T, Davisson MT (2003) Quantitative PCR genotyping assay for the Ts65Dn mouse model of Down syndrome. Biotechniques 35(6), 1170–1174

13. Livak KJ (1997) Comparative *Ct* Method. ABI PRISM 7700 Sequence Detection System, User Bulletin No. 2, Relative quantitation of gene expression. PE Applied Biosystems, http://docs.appliedbiosystems.com/pebio-docs/04303859.pdf

14. Luche RM, Maiwald R, Carlson EJ, Epstein CJ (1997) Novel mutations in an otherwise strictly conserved domain of CuZn superoxide dismutase. Mol Cell Biochem 168, 191–194

15. Lyle R, Gehrig C, Neergaard–Henrichsen C, Deutsch S, Antonarakis SE (2004) Gene expression from the aneuploid chromosome in a trisomy mouse model of Down syndrome. Genome Res 14(7), 1268–1274

16. Pulsifer MB (1996) The neuropsychology of mental retardation. J Int Neuropsychol Soc 22, 159–176

17. Reeves RH, Irving NG, Moran TH, Wohn A, Kitt C, et al. (1995) A mouse model for Down syndrome exhibits learning and behavioral deficits. Nat Genet 11, 177–184

18. Ruiz–Ponte C, Loidi L, Vega A, Carracedo A, Barros F (2000) Rapid real-time fluorescent PCR gene dosage test for the diagnosis of DNA duplications and deletions. Clin Chem 46(10), 1574–1582

19. Sago H, Carlson EJ, Smith DJ, Kilbridge J, Rubin EM, et al. (1998) Ts1Cje, a partial trisomy 16 mouse model for Down syndrome, exhibits learning and behavioral abnormalities. Proc Natl Acad Sci USA 95(11), 6256–6261

20. Sago H, Carlson EJ, Smith DJ, Rubin EM, Crnic LS, et al. (2000) Genetic dissection of the region associated with behavioral abnormalities in mouse models for Down syndrome. Pediatr Res 48(5), 606–613

21. Schaeffeler E, Schwab M, Eichelbaum M, Zanger UM (2003) CYP2D6 genotyping strategy based on gene copy number determination by TaqMan real-time PCR. Hum Mutat 22(6), 476–485

22. Wilke K, Duman B, Horst J (2000) Diagnosis of haploidy and triploidy based on measurement of gene copy number by real-time PCR. Hum Mutat 16(5), 431–436